Linearizing the vertical scale of an interferometric microscope and its effect on step-height measurement

Thomas A. Germer, T. Brian Renegar, Ulf Griesmann, and Johannes A. Soons

Sensor Science Division
National Institute of Standards and Technology
Gaithersburg, Maryland 20899 USA

Email: thomas.germer@nist.gov

Keywords: microscope, linearization, interferometer, calibration, step-height, coherence scanning interferometer

Abstract

The vertical scale calibration of an interferometric microscope is important for establishing traceability of surface topography measurements to the International System of Units (SI) unit of length, the meter. Building on the calibration procedure for the amplification coefficient developed by de Groot and Beverage [Proc. SPIE **9526**, 952610 (2015)], this paper describes a calibration procedure that yields the response curve for the entire vertical scan motion of a coherent scanning interferometric microscope. The method requires only a flat mirror as an artifact, a narrow band spectral filter, an aperture to reduce the effective numerical aperture, and the ability to raise and lower the microscope head so that the center of the interferogram can be varied within the scan range. The local frequency of the interferogram is determined by fitting sections of the interferogram to a sinusoidal function. The nonlinearity determined from the local frequency data can be used to estimate the uncertainty in uncorrected vertical height measurements. We describe how optical profile data can be corrected for nonlinearity due to dynamic effects in the scan motion and show that the correction improves the reproducibility of step height measurements by at least a factor of three and close to that of the repeatability.

---

1. Introduction

Coherent scanning interferometry (CSI), also referred to as white-light interferometry (WLI), is increasingly used for non-contact optical measurement of areal surface topography.[1-5] In CSI imaging, a broadband source is used in conjunction with an interferometric microscope objective (e.g., Michelson or Mirau). A scanning motion, typically of the objective, is used to change the relative path length. The short coherence length of the source yields a narrow interferometric burst for the surface patch near zero path length difference. In most situations, this burst can be resolved for phase very accurately, yielding a precise measure of the surface height, which doesn't suffer from the phase unwrapping problem associated with narrow-band sources used in phase shifting interferometry (PSI).[6] In addition, knowledge of the obliquity factor,[7] which is

required for PSI imaging and which accounts for the mean wave vector normal to the surface, is not required.

In all scanning microscopes, the displacement of the scanning stage, typically a piezoelectric stage, needs to be known, and calibration is required to ensure the traceability of measurements to the SI meter. Calibration of the linear component, the amplification coefficient [8-10], is often performed using a calibrated physical artifact, typically a step-height standard. De Groot and Beverage proposed a method for performing an absolute calibration of the amplification coefficient for interferometric microscopes that does not require a step-height standard.[11] In their method, a narrow-band spectral filter is inserted into the illumination path, the effective numerical aperture of the objective is reduced, and the interferometric objective is used with an optical flat in the sample position as a Fourier transform spectrometer to measure the filter spectrum at the sample location. Comparison of the spectrum obtained in this fashion with that obtained with a calibrated grating spectrometer allows the scale of the latter to be transferred to the microscope.

In addition to the amplification coefficient, linearity of the scanning motion needs to be assessed. The default method in ISO 25178-700 [12] to assess this metrological characteristic is to measure different calibrated step heights, realized by one or more physical artifacts, each at different locations in the scanning range. The linearity deviation is then obtained as the maximum observed deviation of the step height measurement values to their respective calibrated values, after compensation for the estimated error in the vertical axis amplification coefficient. Artifacts representing different step heights, or artifacts incorporating a staircase of heights, can be used to estimate the actual instrument response curve that describes the relation between measured and nominal relative surface heights [10, 13, 14]. Kiyono et al. [15] describe an alternative approach that involves stepping a step height artifact though the scanning range. Bauer et al. [16] extend this approach to larger scanning intervals and lessen the requirement of precise steps, using an artifact incorporating multiple step heights, all sharing the same reference surface. A different category of methods, used for e.g., stylus instruments, involves measurement of an inclined precision flat [8, 12, 15, 17-19]. Errors due to the artifact flatness can be attenuated by also measuring the artifact in its leveled location or through reversal [8, 18]. The advantage of these methods is that they yield a continuous calibration curve for non-linearity. However, for interferometric systems, application of an inclined flat is limited to small tilt angles [12], and hence small scanning ranges, to avoid high fringe densities and retrace errors. Kiyono et al.[15] address this challenge by stepping the inclined flat through the scanning range. A third category of methods [12, 15, 19] relies on an external calibrated displacement measurement system, such as a displacement interferometer or capacitance gauge. Eifler et al. [20] proposed a different approach to estimate the response curve by comparing the calibrated height distribution of a roughness artifact with the measured height distribution. Finally, Zhukova et al. [21] describe an in-situ estimation of the non-linear component of the response function from the differences in two measurements of a sample topography, separated by a known displacement in vertical direction.

In this paper, we describe a calibration approach for linearity deviations where variations in displacements are determined by evaluating the local variation in the interferogram frequency, yielding a continuous measurement of displacement and its deviation from linearity. Any instrument equipped to perform the calibration described by de Groot and Beverage is equipped to perform this continuous calibration. In addition, laser-based interferometers can be calibrated using the technique described.

This paper is organized as follows. In Section 2, we describe the coherent scanning interferometric microscope used in these measurements. Section 3 reviews the estimation of the vertical amplification coefficient as described by de Groot and Beverage using the extended interferogram. Section 4 then describes the fitting of sections of the interferogram to a sinusoid yielding a local frequency. Because the quality of the local frequency determination varies through the interferogram, Section 5 shows how fits obtained at different sample offsets can be combined to address the full scan range. Then, in Section 6, we describe how the local frequency can be used to yield the linear and nonlinear components of the displacement function. In Section 7, we evaluate the effect that the nonlinearity would have on the measurement of different step heights to estimate uncertainty in uncorrected step height measurements. Then, in Section 8, we describe measurements of the displacement function when a smaller scan length is used, showing dynamic effects in the scan motion. In Section 9, we show how observed nonlinearities can be corrected. We finally summarize our results in Section 10.

2. The Instrument

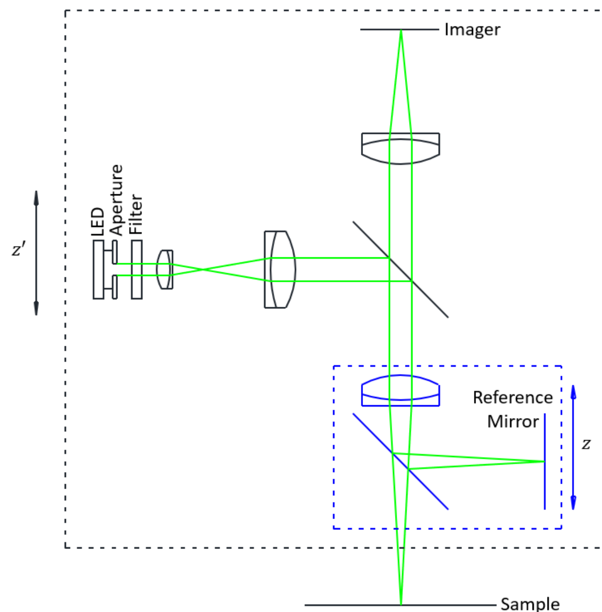

Figure 1 Schematic of the interferometric microscope during calibration. The Michelson interferometric objective, indicated by the inner blue dashed rectangle, moves in the indicated direction under piezoelectric control with coordinate z. The parts in the outer black dashed rectangle move along the same axis for coarse height adjustment with coordinate z'. The filter and aperture are removed during normal operation.

Figure 1 shows a schematic of the interferometric microscope (Zygo Nexview NX2, see disclaimer), modified to enable the in-situ calibration of the vertical amplification coefficient.[11] For these measurements, we use a 5.5x Michelson interferometer objective with a numerical aperture NA = 0.15. During calibration, a 3 nm narrow-band spectral filter is inserted in the illumination path, and the effective NA of the objective is reduced by an illumination aperture conjugate to the back focal plane of the objective. In normal CSI mode, the filter and aperture are removed. The centroid wavelength of the light passing through the objective is measured with a spectrometer referenced to the 546.075(1) nm Hg spectral line and found to be 547.090(10) nm.[22] (Throughout this paper, numbers in parentheses represent standard uncertainties with 68 % confidence intervals and refer to the corresponding last digits in the result.) Interferograms are collected by moving the objective indicated by the inner blue dashed rectangle in Fig. 1 along coordinate z with a piezoelectrically-driven flexure stage with closed-loop capacitive gauge feedback. The range of coordinate z is approximately 150 μm. The microscope contained in the outer black dashed rectangle in Fig. 1 can also be moved with respect to the sample along coordinate z', allowing for different sample thicknesses, coarse focusing, and extended height measurements.

During a single full-range measurement scan, the temporal interferograms are sampled at 2100 discrete points, denoted by ζ, and begin at the top of the scanning motion. The actual objective height is given by $z = h(\zeta)$. Ideally, $h(\zeta) = z_s(2099 - \zeta)$, where z_s is the step distance and $z = 0$ corresponds to the end of the scan at $\zeta = 2099$.

3. Calibration of the Amplification Coefficient

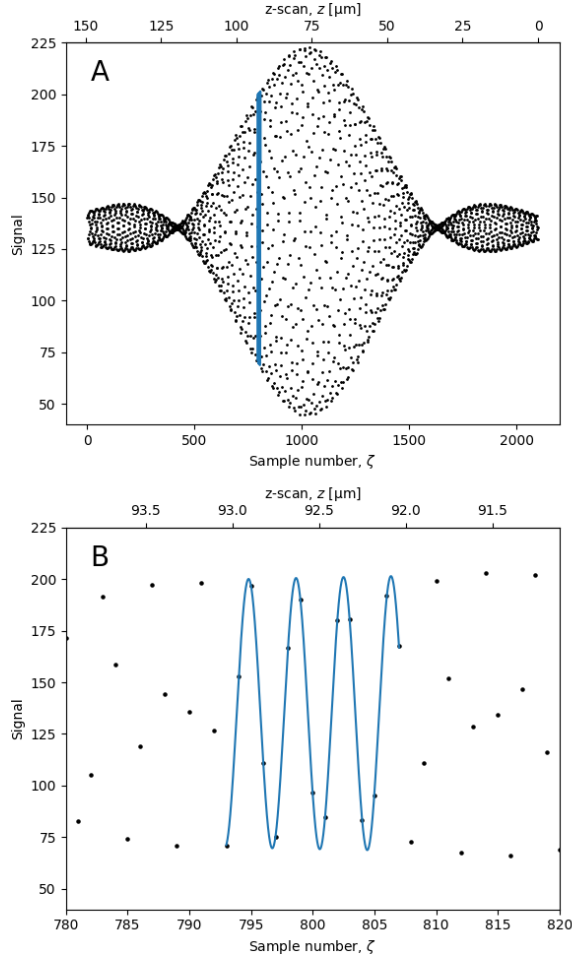

Figure 2 Interferogram measured for a 3 nm wide spectral filter (black points) and a fit to Eq. (3) of 15 sampled data points centered on ζ=800 (blue curve). (A) The entire interferogram, and (B) a section of the interferogram showing the fit.

Using the Michelson interferometer objective with this light source enables calibration of the vertical motion by varying objective height z with respect to a highly polished and flat SiC mirror.[11] Figure 2 shows the interferogram obtained in this fashion averaged over a small 42 × 42 pixel region at the center of the field. The interferogram shows a broad central envelope with side lobes, demonstrating a characteristic coherence length of roughly 100 µm (twice the width of the central lobe), but with measurable degree of partial coherence extending beyond the scan range. The envelope is sinc-like, since the filtered spectrum is approximately rectangularly shaped. The method in [11] for calibrating the amplification coefficient in z calls for performing a Fourier transform of the spectrum to yield a centroid frequency f (in units of inverse steps). The step increment is then given by

$$z_s = \frac{\Omega \lambda_0 f}{2}, \tag{1}$$

where Ω is the obliquity factor, and λ_0 is the centroid wavelength of the 3 nm filtered light measured with the spectrometer. For a small numerical aperture, A_{N}, the obliquity factor is well-approximated by [7]

$$\Omega \cong 1 + \frac{A_{\mathrm{N}}^2}{4} + \frac{A_{\mathrm{N}}^4}{8}. \tag{2}$$

The waveform is nominally sampled with approximately four points per period, so the frequency f is typically about 0.25. The centroid frequency obtained from the Fourier transform is $f =$ 0.260 118(65). We measured the effective NA of the aperture-limited objective to be $A_{\mathrm{N}} =$ 0.041 1(6) by placing a camera under the objective and measuring the diameter of the illuminated area as a function of distance while using a small field stop. Thus, the obliquity factor is 1.000 422(12), and the average step increment is z_{s} = 71.184(18) nm.

4. Local Frequency Measurement

The analysis described above assumes that the z motion is linear, i.e., that z_{s} is constant during a scan. In this paper, we measure the nonlinearity along the z coordinate by fitting small sections of the broad interferogram to a sinusoidal function to obtain the local frequency and evaluating that frequency through the entire interferogram. The function we use when the region is centered on index ζ is a sinusoidal function with a simple linear envelope,

$$S(\zeta_i) = A[1 + a(\zeta_i - \zeta)]\cos[2\pi f(\zeta_i - \zeta) + \phi] + B, \tag{3}$$

where A is the amplitude at ζ, a is the local linear slope of the envelope, f is the local frequency, ϕ is the phase, B is the background, and ζ_i are indices centered on and near ζ. Figure 2 shows a local fit to 15 points about the point $\zeta = 800$. Higher order terms to the envelope were not found to be necessary, provided the number of points in each fit was sufficiently small. The local frequency estimates were relatively independent of the number of points used, until the number of points was greater than about 25, after which the results become smoother. This smoothening is believed to be due to an averaging of oscillations in the local frequency, which were observed to have a period of approximately 29 sample steps. The quality of the fit was determined by the standard deviation of the residuals normalized by the amplitude A and was used for weighted averaging of multiple measurements.

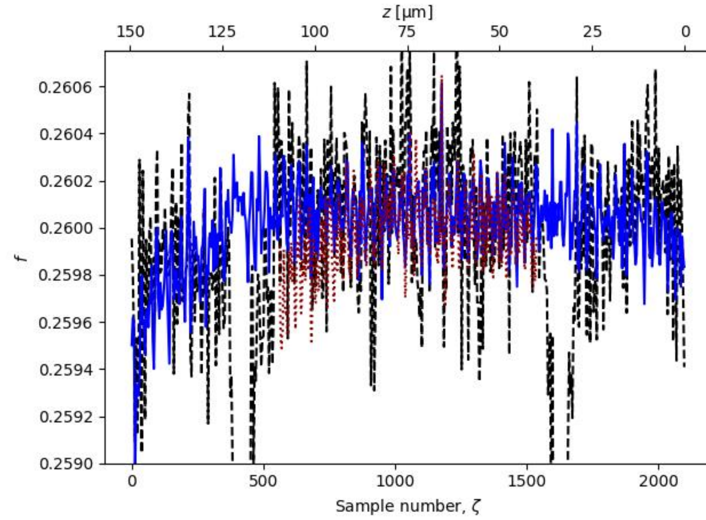

Figure 3 The local frequency of the interferogram measured with a 3 nm spectral filter shown as functions of sample number ζ (bottom scale) and position z (top scale). The curves are: (dashed black curve) the local frequency for a single 150 μm interferogram centered on the data set, (solid blue curve) the weighted average of the local frequency for 150 μm interferograms centered at different locations, and (dotted red curve) the respective results obtained for the 70 μm reduced-length scans. The size of the fit window was 15 points.

The black dashed curve in Fig. 3 shows the local frequency measured from the interferogram shown in Fig. 2. Near the envelope minima, the fits are relatively poor, and the frequency shifts substantially. Between those features, from $\zeta = 600$ to $\zeta = 1500$, the frequency is relatively flat, albeit with some structure (discussed later in Sec. 8). There is a significant decrease in local frequency at the beginning of the scan ($\zeta < 350$) and possibly a smaller decrease at the end of the scan ($\zeta > 1950$).

5. Expanding Local Frequency Measurements

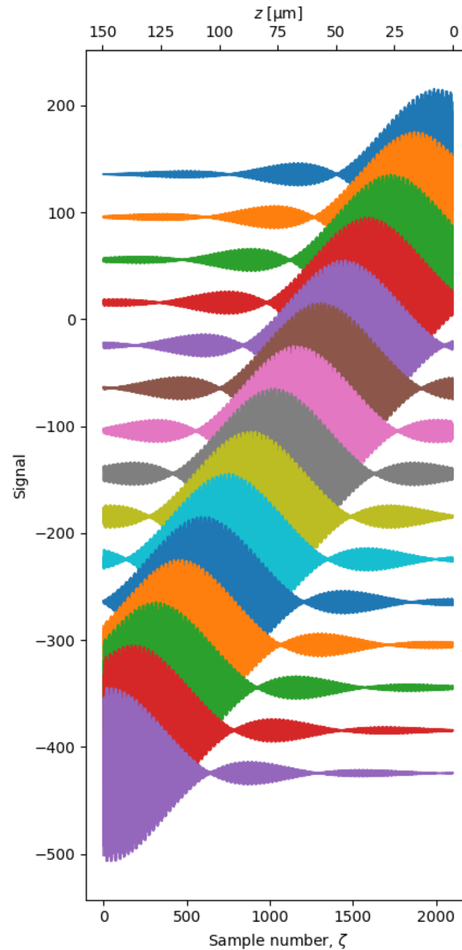

Figure 4 Interferograms measured for a 3 nm spectral filter for different microscope heights z'. The z' heights are shifted in increments of 10 µm. The interferograms are shown vertically offset from each other for clarity. The horizontal scales are sample number ζ (bottom scale) and position z (top scale).

The dashed black curve shown in Fig. 3 is not suitable for calibrating the vertical scale for the entire scanning motion, because the confidence in the local frequency estimates varies over the scan range, with high uncertainties where the interferogram envelope has a minimum. In order to homogenize and improve the uncertainty in the local frequency over the entire range of scanner motion, we performed repeated measurements of the interferogram, with the coarse z' stage stepped in 10 µm increments over the entire z-axis scan range. In this manner, every point along z has an interferogram with its maximum amplitude near it. Figure 4 shows some of the interferograms. We collected interferograms as shown in Fig. 4, with z' stepping in both directions and the sequence repeated 20 times. Each time after moving the coarse z' stage, we waited 30 s to allow the motion to settle, since any motion of this stage would negatively impact the results. We made steps in both directions to improve the balance in any residual settling. There were 600 interferograms measured (15 steps × 2 directions × 20 repeats). Of these 600, only 557 were saved, since the software sometimes reported an error at the z' extremes. The

acquisition was automated, and the total time for all the measurements was approximately 7 hours.

The solid blue curve in Fig. 3 shows the estimated local frequencies, each representing the weighted average of the respective local frequency values obtained at different values of z'. The respective weights are the inverse variance of the local residuals for each fit, normalized by the local amplitude A. Only those parts of the interferogram where the modulations were at least 0.20 of the background were included in the average. To evaluate the repeatability in our results, a bootstrapping analysis was performed, where the whole of the data was divided into subsets and standard deviations of the means of the derived quantities were determined. The solid blue curve in Fig. 3 provides a continuous measure of the local frequency, eliminating the features where the fits are poor for a single interferogram.

6. Determining the Vertical Scale Calibration from Local Frequency

The solid blue curve shown in Fig. 3 can be used to determine the vertical scale of the z motion, comprising a linear term (amplification coefficient) governed by the average frequency $\langle f \rangle$ and a linearity deviation. [8, 9] Recognizing that $\mathrm{d}h(\zeta)/\mathrm{d}\zeta$ is the negative local step distance, $-z_{\mathrm{s}}(\zeta)$, the local frequency $f(z)$ we measure is related to the centroid optical wavelength λ_0 and the obliquity factor Ω by [see Eq. (1)]

$$\frac{\Omega\lambda_0 f(\zeta)}{2} = -\frac{\mathrm{d}h(\zeta)}{\mathrm{d}\zeta}. \tag{4}$$

The negative sign in Eq. (4) results from the motion starting from the top. We can integrate Eq. (4) to obtain the position function

$$h(\zeta) = c - \frac{\Omega\lambda_0}{2}\int f(\zeta)\,\mathrm{d}\zeta\,, \tag{5}$$

where c is the integration constant. The integral can be approximated by a sum

$$h(\zeta) \cong c - \frac{\Omega\lambda_0}{2}\sum_{\zeta_i=\zeta_0}^{\zeta} f(\zeta_i)\Delta\zeta\,, \tag{6}$$

where ζ_0 is the beginning of the scan and $\Delta\zeta$ is the step increment over which the fits were performed. Eq. (6) can be rewritten as

$$z = h(\zeta) = c - z_{\mathrm{s}}\zeta - z_{\mathrm{NL}}(\zeta), \tag{7}$$

where

$$z_{\mathrm{s}} = \beta\langle f \rangle, \tag{8}$$

$$z_{\mathrm{NL}}(\zeta) = \beta\sum_{\zeta_i=\zeta_0}^{\zeta} \Delta f(\zeta_i)\Delta\zeta\,. \tag{9}$$

$$\Delta f(\zeta) = f(\zeta) - \langle f \rangle, \tag{10}$$

$$\beta = \frac{\Omega \lambda_0}{2}, \tag{11}$$

The first term, the integration constant c, corresponds to an overall offset of the z-stage and is not important for differential measurements (e.g., roughness, step heights, etc.). The second term represents the linear behavior of the z-stage. The third term represents the nonlinearity. The average frequency $\langle f \rangle$ can be computed in different ways:

- One method is to average over the entire scan length. In this case, the linear term is the line through the end points of the z-axis response function, and the nonlinearity is zero at the two ends. The $\langle f \rangle$ calculated this way is $\langle f \rangle_1 = 0.260\,006$.
- A second method uses the slope of the linear regression line through the z-axis response curve, following the definition of the amplification coefficient in the ISO standard. [8, 9] The $\langle f \rangle$ calculated this way is $\langle f \rangle_2 = 0.260\,048$. With this method, the nonlinearity component is minimized over the entire scan range in a least-squares sense.
- A third method is to use the centroid frequency determined from the Fourier transform of the centered interferogram. This value $\langle f \rangle$ was reported earlier and is $\langle f \rangle_3 = 0.260\,118(65)$. This method is incorporated by the built-in instrument software.
- A final method is to choose a region in the middle of the z-scan, where the frequency is relatively constant. With this method, used in the remainder of this paper, the nonlinearity in the center region will be minimized. The $\langle f \rangle$ determined in this way is $\langle f \rangle_4 = 0.260\,071$. The result of this method is close to that of the third method, as the latter method also averages the local frequency in the center region due to the envelope acting as a weighting function.

In all cases, the choice of the method for determining $\langle f \rangle$ does not affect the calibration curve obtained, but instead determines its separation into a linear component and a nonlinear component. The respective choice can be important when the instrument only allows for compensation of the linear component.

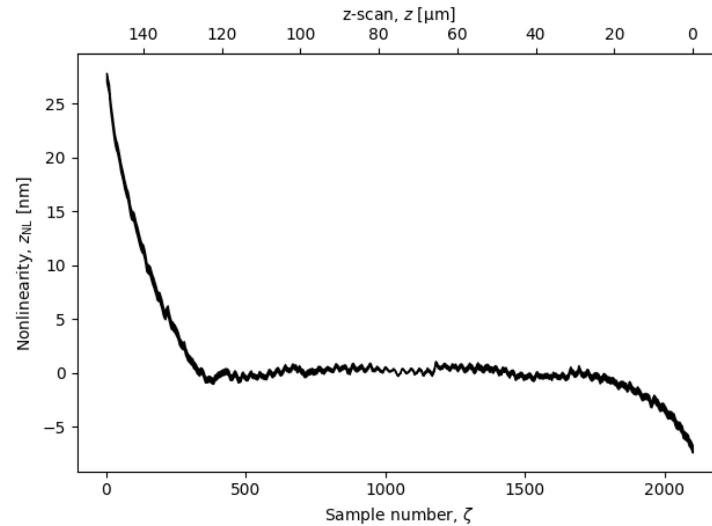

Figure 5 The nonlinearity determined for a full 150 µm scan length, with 2100 data points. The horizontal scales are sample number ζ (bottom scale) and position z (top scale). The line width of the curve represents the standard deviation of the mean, estimated using a bootstrap analysis of subsets of the entirety of the data.

Figure 5 shows the nonlinearity obtained from the results shown in Fig. 2 (solid curve), where the mean frequency was estimated from the central half of the scan length (the fourth method describe above). The nonlinearity curve is relatively flat from 400 to 1700 (or z from 25 µm to 125 µm), but there is a significant nonlinearity outside this range. We will discuss possible sources of nonlinearity later in Sec. 8.

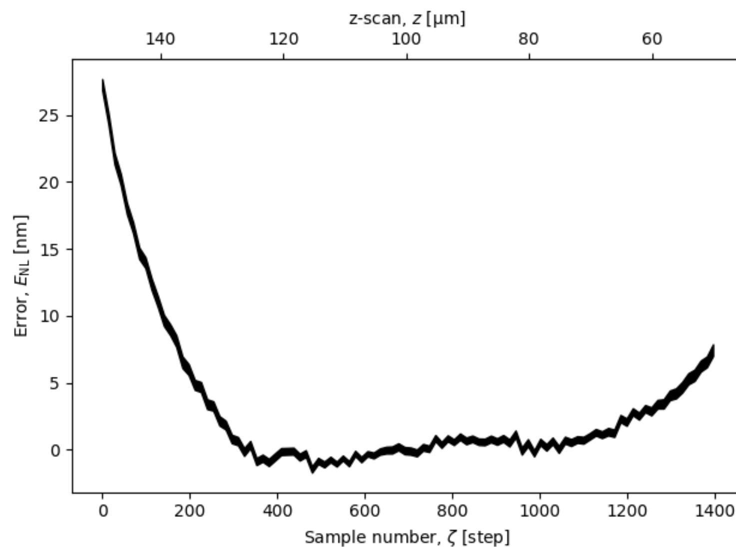

Figure 6 The estimated error for the measurement of a 50 µm step height measured at various locations in the scan range. The abscissa represents the location of the top surface

of the step in units of sample number ζ (lower scale) and position z (upper scale). The line width of the curve represents the standard deviation of the mean of the estimated error estimated using a bootstrap analysis of subsets of the entirety of the data.

7. Step Height Errors

Nonlinearity will affect the measurement of a step height artifact. In the following, we estimate its contribution to the uncertainty, if the z scale is not corrected to address the nonlinearity. Here the corrected linear term is estimated using the fourth method described above. If the height of the step is H, the error from nonlinearity would be

$$E_{\mathrm{NL}}(z_{\mathrm{top}}) = z_{NL}(z_{\mathrm{top}}) - z_{NL}(z_{\mathrm{top}} - H), \tag{12}$$

where z_{top} is the z scan height of the top surface of the step. Figure 6 shows the expected error if a 50 μm step were measured, with the top surface of the step positioned at various locations in the scan range. If the top and bottom surfaces of the step are centered in the scan range, then the error from nonlinearity is relatively small. However, if either the top or bottom surfaces of the step are near the extremes of the scan range, the error grows significantly. We presume that the operator can easily position the step height artifact within the center half of the curve shown in Fig. 6. We then evaluate the standard uncertainty due to uncorrected nonlinearity as the root-mean-square of the central portion of the curve shown in Fig. 6. We choose to use the root-mean-square because it adds the standard deviation and offsets in quadrature.

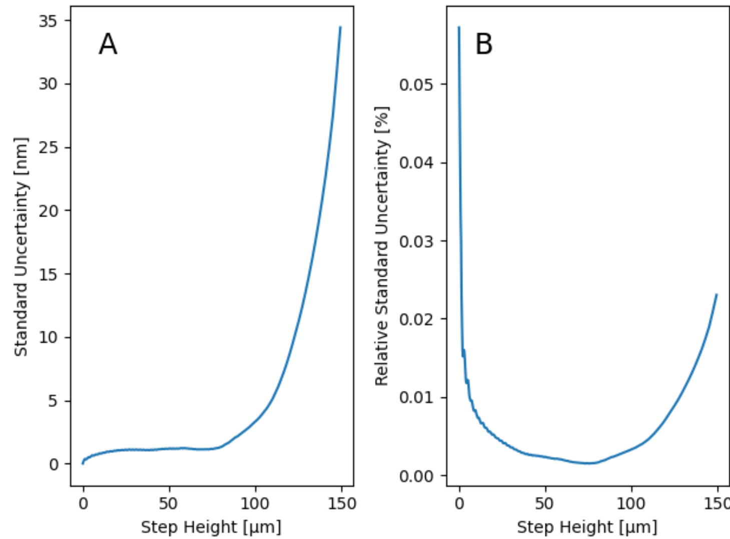

Figure 7 (A) The simulated standard uncertainty of a step height measurement due to scan nonlinearity, when the step is kept within half of its permissible scan range, and (B) the same as a fraction of the step height.

Figure 7 shows the estimated standard uncertainty and the relative standard uncertainty evaluated as described as a function of the step height. At small step heights, less than about 75 μm, the uncertainty is dominated by the fluctuations observed in the central section of the nonlinearity curve. At step heights larger than about 75 μm, the nonlinearity at the ends of the z scan contributes to an offset in the measured value. For these larger steps, the range of the coarse z' stage positions for which the top and bottom surfaces are in the scan range is smaller. A more careful centering of the artifact in the z scan range may help to reduce the estimated uncertainty, but only to a limited extent, since the error for larger step heights is dominated by that offset. The relative uncertainty shown in Fig. 7(b) rises to nearly 0.025 % for large step heights. For small step heights, the maximum uncertainty from nonlinearity approaches about 0.055 %.

8. Sources of Nonlinearity

Nonlinearity can arise from multiple sources. While we are not privy to some details of the operation of the commercial microscope, the z stage is a closed-loop piezoelectric actuator flexure stage with capacitance gauge feedback. Static and dynamic effects can contribute to nonlinearity.

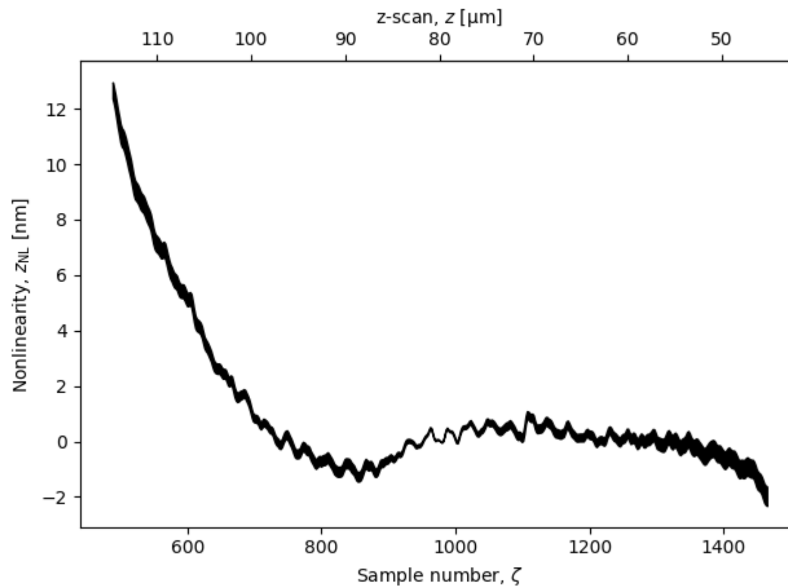

Figure 8 The nonlinearity measured for a 70 μm scan length, with 977 data points. The horizontal scales are sample number ζ (bottom scale) and position z (top scale). The line width of the curve represents the standard deviation of the mean estimated using a bootstrap analysis of subsets of the entirety of the data.

To help assess the origin of the nonlinearity, we performed the same measurements described above, but using a shorter 70 μm scan length (977 samples). The scan starts at location $\zeta = 561$ of the 2100 data point total scans. Figure 3 (red, dashed curve) shows the local frequency values extracted from the interferograms for the 70 μm scan length. Figure 8 shows the resulting nonlinearity. The nonlinearity at the start of the scan ($\zeta = 561$) mimics that at the start of the scan in Fig. 5 ($\zeta = 0$). This result suggests the presence of acceleration effects at the beginning

of a scan that result in variations in the spatial separation of points in the acquired interferogram signal.

Close examination of the results in Fig. 3 shows that there is an oscillation in the local frequency with an approximate period of 30 steps and that the oscillations are synchronous in ζ between all the three data sets. In addition, the amplitude in the frequency oscillations obtained from a single interferogram (black dashed curve, outside the two regions where the frequency deviates strongly from the other data) is nearly the same as that for the weighted average over the 577 interferograms. We conclude that these oscillations are not random and that they are not caused by systematic effects in the fitting procedure. We suspect there is a periodic variation in the velocity of the z scan that is fixed with respect to the stage coordinate. One possible cause is that the stage position is being servoed to a voltage provided by a digital-to-analog converter with a finite resolution. In fact, many flexure stages have resolutions in the few-nanometer range. The fine structure in the nonlinearity (see Figs. 5 and 8) is of that magnitude.

9. Vertical scale correction

The stability of the curves shown in Figs. 5 and 8 suggests that the accuracy of the measured nonlinearity function $z_{\mathrm{NL}}(\zeta)$ is high for each scan range, and that it can be used to correct measurement data. When one performs a local height analysis, say as described by de Groot, [1] the resulting height data could be kept in step coordinates ζ, followed by an interpolation of Eq. (7) to convert the step levels (including fractions thereof) to height. Earlier, we discussed several methods for determining $\langle f \rangle$. Eq. (7) is invariant to the choice of $\langle f \rangle$, so, in principle, once this calibration is performed, the $h(\zeta)$ function is fully calibrated over the entire height range for a particular choice of scan range.

We performed measurements of two different step height artifacts, one nominally 23 µm and one nominally 50 µm, in different regions of the scan range. The chosen scan range equaled the full 150 µm available, which corresponds to that of Fig 7. The sequence of measurements was performed by stepping z' in one direction and then in the other, yielding two mean step height values for each z'. For each z', 8 interferograms were acquired and saved, each separated in time by 5 s to ensure that the instrument stabilized. (Preliminary measurements used the instrument's automated repeat scanning feature, which acquires multiple interferograms in rapid succession. However, the analysis described here did not perform as well, possibly because residual vibrations did not replicate those measured during the calibration procedure.) Interpretation of the interferograms and reduction to uncorrected heights z_{u} was performed by the manufacturer's software. The effective sample number is $\zeta = z_{\mathrm{u}}/z_{\mathrm{s,u}}$, where the step increment $z_{\mathrm{s,u}}$ is provided by the most recent instrument calibration (available in the measurement metadata). Eq. (7) can then be used to find the corrected height

$$z_{\mathrm{c}} = c + z_{\mathrm{s}} z_{\mathrm{u}}/z_{\mathrm{s,u}} + z_{NL}\left(z_{\mathrm{u}}/z_{\mathrm{s,u}}\right). \qquad (13)$$

Finally, the uncorrected and corrected height maps were analyzed for step height by choosing two regions, A and B corresponding to the bottom and top surfaces of the respective step. A least squares fit was performed of the data to the function

$$h(x,y) = \begin{cases} h_0 + m_x x + m_y y & (x,y) \in A \\ h_0 + m_x x + m_y y + H & (x,y) \in B \end{cases}. \quad (13)$$

Here, m_x and m_y are slopes in the x and y directions due to sample tilt, respectively, h_0 is the position of the lower region, and H is the step height. These fits are performed for both the uncorrected height z_u and the corrected height z_c.

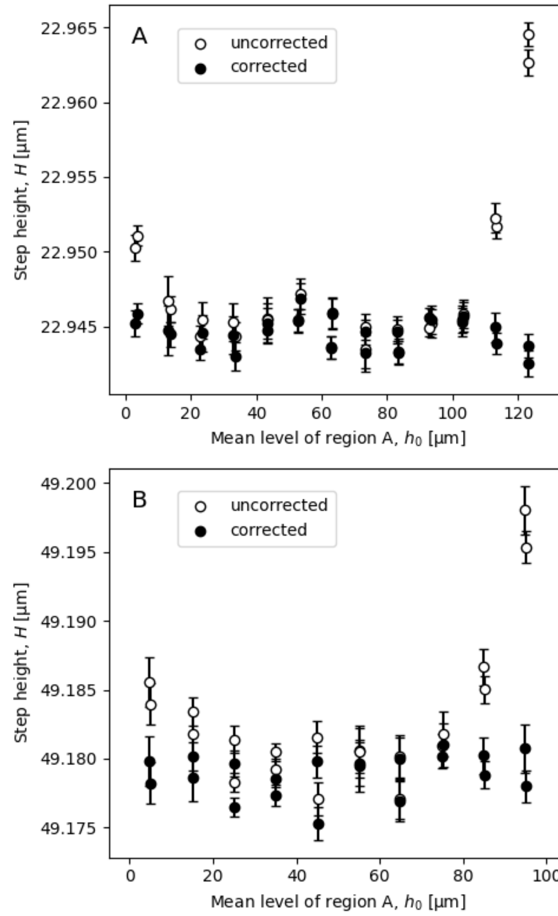

Figure 9 Uncorrected (open circles) and corrected (closed circles) step heights determined from a nominal 23 µm step height artifact (A) and a nominal 50 µm step height artifact (B) as functions of the mean level of the step height top surface in the scanner range. The error bars represent the standard deviation of the mean of 8 repeated measurements.

Table 1 Summary of data shown in Fig. 9.

H	$\langle u \rangle$	σ(uncorrected)	σ(corrected)
23 µm	0.9 nm	5.8 nm	1.1 nm
50 µm	1.3 nm	5.2 nm	1.5 nm

Figure 9 shows the results of this analysis, and a summary is given in Table 1. The error bars u shown in Fig. 9 reflect the standard deviation of the mean of 8 repeated measurements. In Table 1, $\langle u \rangle$ represents the mean value of these standard deviations. In the case of the 23 μm step height artifact, the standard deviation σ of the results was reduced from 5.8 nm to 1.1 nm, while for the 50 μm step height, the standard deviation σ of the results was reduced from 5.2 nm to 1.5 nm. A sharp rise in measured step height, observed in the uncorrected results at both ends of the range, is removed by the correction procedure. There are no substantial trends remaining in the step heights, although the results for the 23 μm step height may indicate a residual component periodic with sample position. The standard deviations of the corrected data, $\sigma(\text{corrected})$, are only slightly higher than the mean estimated standard deviation of the data for each height measurement, $\langle u \rangle$, suggesting that most of the nonlinearity of the instrument was removed by the proposed calibration method.

10. Summary

We describe a new method to determine the vertical height scale of an interferometric microscope. The method is straightforward to perform using the functionality of current commercial instruments. By performing a local determination of the interferogram frequency, rather than working in the Fourier domain to obtain a single centroid frequency, this method enables the estimation and correction of systematic linearity errors, including those due to system dynamics. Our results show that system dynamics can cause the nonlinearity to depend upon the choice of scan range. While the method as applied in this study is relatively time-consuming, both with data collection and computation, it yields the nonlinearity with high resolution, provides information about the system stability and reproducibility, and is fully automated. We demonstrate improved performance using two step height artifacts measured at different locations within the scan range.

Data Availability

All the original data for this paper and the code used to analyze them are available for download at https://doi.org/10.18434/mds2-3116.

Conflicts of Interest

The authors have no conflicts of interest to report.

Funding Source

This work was not funded by an external funding source.

Disclaimer

Certain equipment, instruments, software, or materials, commercial or non-commercial, are identified in this paper in order to specify the experimental procedure adequately. Such identification is not intended to imply recommendation or endorsement of any product or service by NIST, nor is it intended to imply that the materials or equipment identified are necessarily the best available for the purpose.

References

[1] P. de Groot, "Principles of interference microscopy for the measurement of surface topography," Adv Opt Photonics **7** (1), 1-65 (2015).
[2] P. de Groot, X. C. de Lega, R. Su and R. Leach, "Does interferometry work? A critical look at the foundations of interferometric surface topography measurement," Proc. SPIE **11102**, 111020g (2019).
[3] R. Su, "Coherence Scanning Interferometry," in *Advances in Optical Surface Texture Metrology*, edited by R. Leach (IOP Publishing Ltd., 2020), pp. 2.1-2.27.
[4] P. De Groot, "Coherence Scanning Interferometry," in *Optical Measurement of Surface Topography*, edited by R. Leach (Springer, 2011), pp. 187-208.
[5] ISO 25178-604:2013, "Geometrical product specifications (GPS) — Surface texture: Areal — Part 604: Nominal characteristics of noncontact (coherence scanning interferometry) instruments," (2013).
[6] P. De Groot, "Phase Shifting Interferometry," in *Optical Measurement of Surface Topography*, edited by R. Leach (Springer, 2011), pp. 167-186.
[7] K. Creath, "Calibration of Numerical Aperture Effects in Interferometric Microscope Objectives," Appl Optics **28** (16), 3333-3338 (1989).
[8] R. Leach, H. Haitjema, R. Su and A. Thompson, "Metrological characteristics for the calibration of surface topography measuring instruments: a review," Measurement Science and Technology **32**, 032001 (2021).
[9] ISO 25178-600:2019, "Geometrical product specifications (GPS) — Surface texture: Areal — Part 600: Metrological characteristics for areal topography measuring methods," (2019).
[10] A. Pappas, L. Newton, A. Thompson and R. Leach, "Review of material measures for surface topography instrument calibration and performance verification," Measurement Science and Technology **35** (1), 012001 (2024).
[11] P. de Groot and J. Beverage, "Calibration of the amplification coefficient in interference microscopy by means of a wavelength standard," Proc. SPIE **9526**, 952610 (2015).
[12] ISO 25178-700:2022, "Geometrical product specifications (GPS) — Surface texture: Areal — Part 700: Calibration, adjustment and verification of areal topography measuring instruments," (2022).
[13] C. L. Giusca, R. K. Leach and F. Helery, "Calibration of the scales of areal surface topography measuring instruments: part 2. Amplification, linearity and squareness," Measurement Science and Technology **23** (6), 065005 (2012).
[14] S. Boedecker, C. Rembe, H. Schmid, T. Hageney and T. Kohnlein, "Calibration of the z-axis for large-scale scanning white-light interferometers," J Phys Conf Ser **311**, 012027 (2011).
[15] S. Kiyono, W. Gao, S. Z. Zhang and T. Aramaki, "Self-calibration of a scanning white light interference microscope," Opt Eng **39** (10), 2720-2725 (2000).

[16] W. Bauer, D. Huser and D. Gerbert, "Simple method to determine linearity deviations of topography measuring instruments with a large range axial scanning system," Precis Eng **64**, 243-248 (2020).
[17] ISO 12179:2021, "Geometrical product specifications (GPS) - Surface texture: Profile method - Calibration of contact (stylus) instruments," (2021).
[18] C. L. Giusca and S. Goel, "Improved and simpler estimation of scale linearity contribution to topography measurement," Precis Eng **60**, 368-373 (2019).
[19] H. Haitjema and M. A. A. Morel, "Accurate roughness measurements by dynamic calibration, VFM-uncertainty calculations and a special calibration specimen," 7th International Symposium on Measurement Technology and Intelligent Instruments **13**, 232-235 (2005).
[20] M. Eifler, F. Schneider, J. Seewig, B. Kirsch and J. C. Aurich, "Manufacturing of new roughness standards for the linearity of the vertical axis – Feasibility study and optimization," Engineering Science and Technology **19**, 1993-2001 (2016).
[21] L. Zhukova, R. Artigas and G. Carles, "Computational self-correction of scanning nonlinearities in optical profilometry," Proc. SPIE **12618**, 126180V (2023).
[22] C. J. Sansonetti, M. L. Salit and J. Reader, "Wavelengths of spectral lines in mercury pencil lamps," Appl Optics **35** (1), 74-77 (1996).